

The debris disc of solar analogue τ Ceti: *Herschel* observations and dynamical simulations of the proposed multiplanet system

S. M. Lawler,^{1,2★} J. Di Francesco,^{1,2} G. M. Kennedy,³ B. Sibthorpe,⁴ M. Booth,⁵ B. Vandenbussche,⁶ B. C. Matthews,^{1,2} W. S. Holland,^{7,8} J. Greaves,⁹ D. J. Wilner,¹⁰ M. Tuomi,^{11,12} J. A. D. L. Blommaert,^{6,13,14} B. L. de Vries,^{15,16} C. Dominik,^{17,18} M. Fridlund,^{19,20} W. Gear,²¹ A. M. Heras,²² R. Ivison^{23,24} and G. Olofsson¹⁵

Affiliations are listed at the end of the paper

Accepted 2014 August 10. Received 2014 August 6; in original form 2014 May 8

ABSTRACT

τ Ceti is a nearby, mature G-type star very similar to our Sun, with a massive Kuiper Belt analogue and possible multiplanet system that has been compared to our Solar system. We present *Herschel Space Observatory* images of the debris disc, finding the disc is resolved at 70 μm and 160 μm , and marginally resolved at 250 μm . The *Herschel* images and infrared photometry from the literature are best modelled using a wide dust annulus with an inner edge between 1 and 10 au and an outer edge at ~ 55 au, inclined from face-on by $35^\circ \pm 10^\circ$, and with no significant azimuthal structure. We model the proposed tightly packed planetary system of five super-Earths and find that the innermost dynamically stable disc orbits are consistent with the inner edge found by the observations. The photometric modelling, however, cannot rule out a disc inner edge as close to the star as 1 au, though larger distances produce a better fit to the data. Dynamical modelling shows that the five-planet system is stable with the addition of a Neptune or smaller mass planet on an orbit outside 5 au, where the radial velocity data analysis would not have detected a planet of this mass.

Key words: planets and satellites: dynamical evolution and stability – planet–disc interactions – circumstellar matter – stars: individual: τ Ceti.

1 INTRODUCTION

Although hundreds of planetary systems are now known, we are still trying to understand whether or not our Solar system is typical. The distributions of known planetary system parameters are strongly affected by observational biases that are not easy to disentangle from the true distributions. Moreover, our Solar system’s architecture (small rocky inner planets, large gaseous outer planets, and an outer debris disc) has not yet been found in other systems, most likely due to these same biases. For example, long time baselines are required to discover planets at greater than a few au by either the transit or radial velocity (RV) techniques, and directly imaging planets around mature stars like τ Ceti (5.8 Gyr; Mamajek & Hillenbrand 2008) is difficult due to the low fluxes of planets after they lose most of their initial heat from formation (e.g. Spiegel & Burrows 2012).

Fortunately, structures in debris discs can indicate the presence of additional planets. Indeed, one planet so far has been predicted based on disc morphology and then later discovered by direct imaging or another technique (β Pic b; Mouillet et al. 1997; Lagrange et al.

2010). In this paper, we use the debris disc to probe the planetary system around τ Ceti.

τ Ceti is a solar-type analogue located only 3.65 pc from the Sun. The infrared excess towards τ Ceti has been known for nearly three decades, first discovered by *IRAS* (Aumann 1985) and later confirmed by *ISO* (Habing et al. 2001).

Greaves et al. (2004), using the Submillimeter Common-User Bolometer Array (SCUBA; Holland et al. 1999) instrument on the James Clerk Maxwell Telescope (JCMT), found τ Ceti to have a significant excess and moderately resolved disc at 850 μm , extending 55 au from the star, and inferred to be misaligned with the rotational axis of the star. They fit the observed excess between 60 μm and 850 μm with a single-temperature blackbody at 60 K, and obtained a disc mass of $1.2 M_\oplus$, about an order of magnitude higher than our Kuiper Belt.

Here, we revisit the τ Ceti disc with higher-resolution far-IR images taken by the *Herschel Space Observatory*,¹ attempting to

¹ *Herschel* is an ESA space observatory with science instruments provided by European-led Principal Investigator consortia and with important participation from NASA.

★E-mail: lawler@uvic.ca

Table 1. *Herschel* observations of τ Ceti.

ObsID	Date	Instrument	Duration (s)
1342199389	2010 June 29	SPIRE 250/350/500	2906
1342213575	2011 January 31	PACS 70/160	5478
1342213576	2011 January 31	PACS 70/160	5478

better constrain the properties of the disc. Additionally, we find the observed disc probably does not overlap with the orbits of the proposed multiplanet system (Tuomi et al. 2013), though we cannot rule out a disc inner edge inside the orbit of the outermost planet.

In Section 2, we present the *Herschel* observations. Section 3 discusses the constraints these observations place on the properties of the τ Ceti debris disc. In Section 4, we show that the disc inner edge inferred from the modelling is compatible with the proposed compact multiplanet system, and we use dynamical simulations to investigate system stability and the possible presence of additional planets. In Section 5 we discuss the τ Ceti disc–planet system in the context of other known solar systems, and a summary of our conclusions is given in Section 6.

2 HERSCHEL OBSERVATIONS

τ Ceti and its surroundings were observed with the *Herschel Space Observatory* (Pilbratt et al. 2010) using both the Photodetector Array Camera and Spectrometer (PACS; Poglitsch et al. 2010) and the Spectral and Photometric Imaging Receiver (SPIRE; Griffin et al. 2010) as part of the Guaranteed Time Key Programme ‘Stellar Disc Evolution’ to study the six most well-known debris discs (PI: G. Olofsson; Proposal ID: KPGT_golofs01_1). Data at 70 μm and 160 μm were obtained simultaneously using the PACS large scan-map mode on 2011 January 31 over a successive scan and a cross-scan each lasting 91.3 min (ObsIDs: 1342213575 and 1342213576). The PACS scan speed was 20 arcsec s^{-1} . Data at 250 μm , 350 μm , and 500 μm were obtained simultaneously in the SPIRE large photometric scanning observing mode (‘SpirePhotoLargeScan’) on 2010 June 29 over one pass lasting 48.4 min (ObsID: 1342199389). The SPIRE scan speed was 30 arcsec s^{-1} (the medium scan rate). Table 1 summarizes the *Herschel* observations.

The PACS and SPIRE data were reduced separately following standard procedures in HIPE version 13 (Ott 2010) using calibration set 65. Table 2 lists the measured fluxes or upper limits for each band. PACS aperture photometry is measured using 12 and 22 arcsec apertures for the 70 and 160 μm bands, respectively. Uncertainties for the PACS photometry values are computed using several apertures on the background. All uncertainties are 1σ . Table 2 also lists the beam sizes for each band (Vandenbussche et al. 2010).

The SPIRE data provide mainly upper limits, as the disc grows fainter and the resolution grows larger as we proceed to longer

Table 2. *Herschel* measurements of τ Ceti.

λ (μm)	Flux (mJy)	Unc. (mJy)	Beam size (arcsec)
70	303	6	5.6
160	111	8	11.3
250	35	10	18.1
350	<28	–	25.2
500	<20	–	36.9

wavelengths. At 250 μm , assuming the disc is not resolved, the flux comes from the peak pixel, which has 24 ± 6 mJy, with the uncertainty coming from confusion. Using the modelling described in Section 3.1.1, we find 35 ± 10 mJy. This is more reliable since the disc may be marginally resolved at 250 μm . At 350 μm there is some emission where τ Ceti is expected to be, which added to the confusion limit gives <28 mJy. At 500 μm , only confusion is visible, giving a limit of <20 mJy.

Photometric calibration uncertainties are expected to be within 3 per cent at 70 μm , 5 per cent at 160 μm , and 15 per cent at 250 μm , 350 μm , and 500 μm (Poglitsch et al. 2010; Swinyard et al. 2010; Müller et al. 2011).

Fig. 1 shows a composite of cropped *Herschel* maps at 70 μm , 160 μm , 250 μm , 350 μm , and 500 μm , centred at a position of 01:44:02.6, $-15:56:05.8$ (J2000), the position of peak emission at 70 μm . This position is within ~ 1 arcsec of the expected position of τ Ceti, given both its ICRS coordinates (i.e. 01:44:04.08, $-15:56:14.9$) and proper motion ($\mu_\alpha = -1.72105$ arcsec yr^{-1} , $\mu_\delta = +0.85416$ arcsec yr^{-1}) from the *Hipparcos* Catalogue (van Leeuwen 2007).

τ Ceti at 70 μm in Fig. 1(a) is bright and quite compact; the three ‘lobes’ located in the NNW, SSW, and ENE directions are artefacts of the PACS beam at 70 μm . Given these secondary beam features, it is not possible to tell by eye if any 70 μm emission is extended. The source at 160 μm in Fig. 1(b) is less bright but still compact. At 250 μm (see Fig. 1c), the source is less significant but the star-centred emission is associated with τ Ceti. At 350 and 500 μm (Figs 1d and e, respectively), any emission at the τ Ceti position is hard to distinguish from the background confusion.

Fig. 2 shows the uncropped *Herschel* maps at each wavelength, stretched in colour to emphasize faint background sources. At 70 μm (Fig. 2a), τ Ceti dominates the image but a few other background sources are seen. Most notably, the extended galaxy MCG-03-05-018 located to the WSW at 01:43:46.8, $-15:57:29$ (J2000) is also detected. Moving to 160 μm (Fig. 2b), τ Ceti is no longer the brightest object seen; MCG-03-05-018 and many other background objects are brighter. Also, more faint background sources are seen. At 250 μm , 350 μm , and 500 μm (Figs 2c, d, and e, respectively), though some emission may be associated with τ Ceti (particularly at 250 μm), it is barely distinguishable from emission of background objects. Note that MCG-03-05-018 is clearly detected in all five *Herschel* bands.

3 τ CETI’S DEBRIS DISC

It is not obvious from Fig. 1 that a disc is present due to large contrast with the star. Therefore, we present peak- and star-subtracted images to highlight the extended disc structure. Fig. 3 shows the images of the flux towards τ Ceti at 70 and 160 μm , where the point spread function (PSF) has been scaled to the value of the peak pixel and subtracted. This makes it clear that there is extended structure around τ Ceti, visible at both 70 and 160 μm . For comparison, Fig. 4 shows the star-subtracted images at the same wavelengths, where the PSF has been scaled to τ Ceti’s photosphere and subtracted; contours give significance of the remaining flux.

Fig. 5 shows the observed flux density distribution (hereafter referred to as spectral energy distribution, SED) of τ Ceti, using data obtained from the literature and *Herschel* (see caption and Table 3 for specific references). Fig. 5 also shows a stellar photosphere model fit to the data. As can be easily seen, the stellar model fits the data from optical to mid-infrared wavelengths (24 μm). At longer (PACS) wavelengths, however, the observed fluxes are

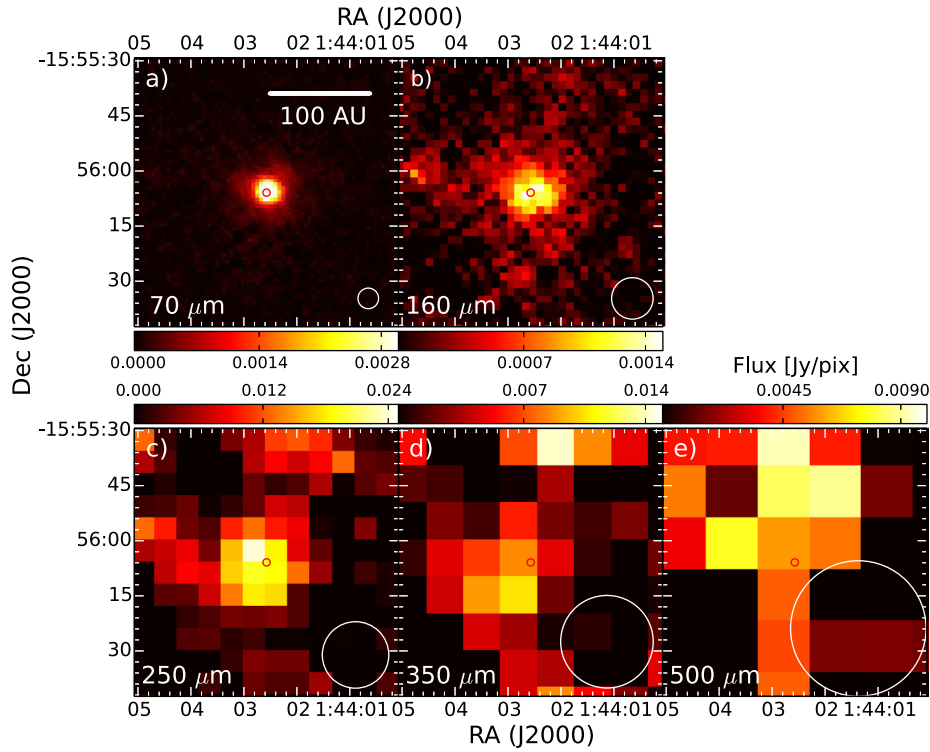


Figure 1. Cropped *Herschel* maps of τ Ceti centred on the position of peak 70 μm emission (shown in each panel as a small red circle). Beam size at each wavelength is shown for reference in each panel (larger white circles). A scale bar showing the colour range of flux in Jy per pixel is shown above each sub-figure. (a) 70 μm emission, (b) 160 μm emission, (c) 250 μm emission, (d) 350 μm emission, and (e) 500 μm emission. A bar in (a) shows the spatial extent of 100 au at the distance of τ Ceti.

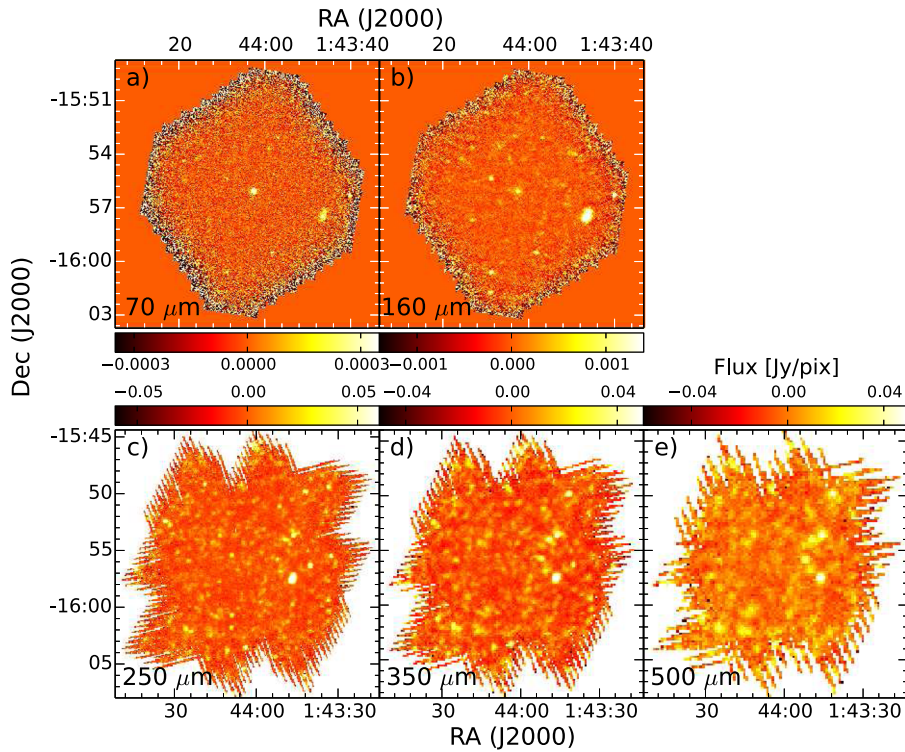


Figure 2. Uncropped *Herschel* maps of the τ Ceti region. A scale bar showing the colour range of flux in Jy per pixel is shown above each sub-figure (a) 70 μm emission, (b) 160 μm emission, (c) 250 μm emission, (d) 350 μm emission, and (e) 500 μm emission.

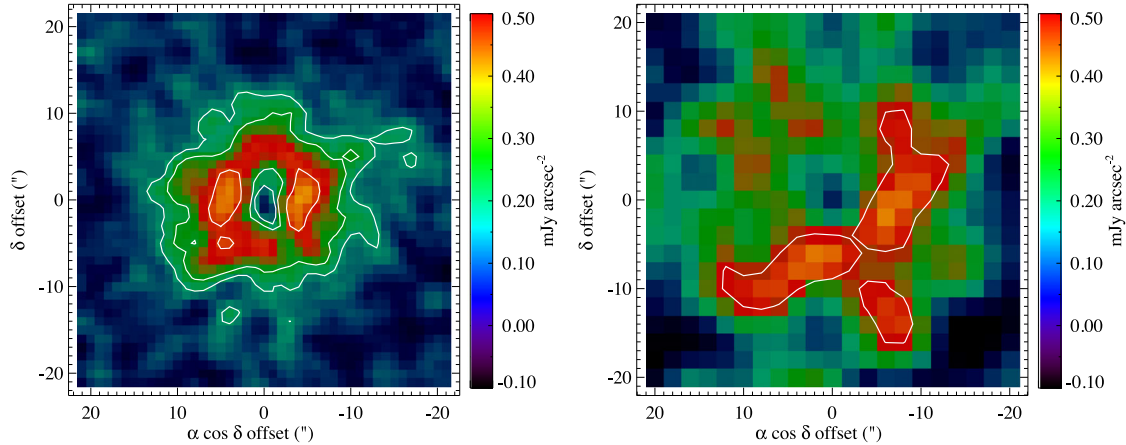


Figure 3. Peak-subtracted images at 70 (left) and 160 μm (right). Here, a PSF has been scaled to the flux of the peak pixel in each band and subtracted from the images (see text for details). Contours show 3σ , 5σ , and 10σ significance levels of the remaining flux (only the 3σ contour is visible in the bottom image).

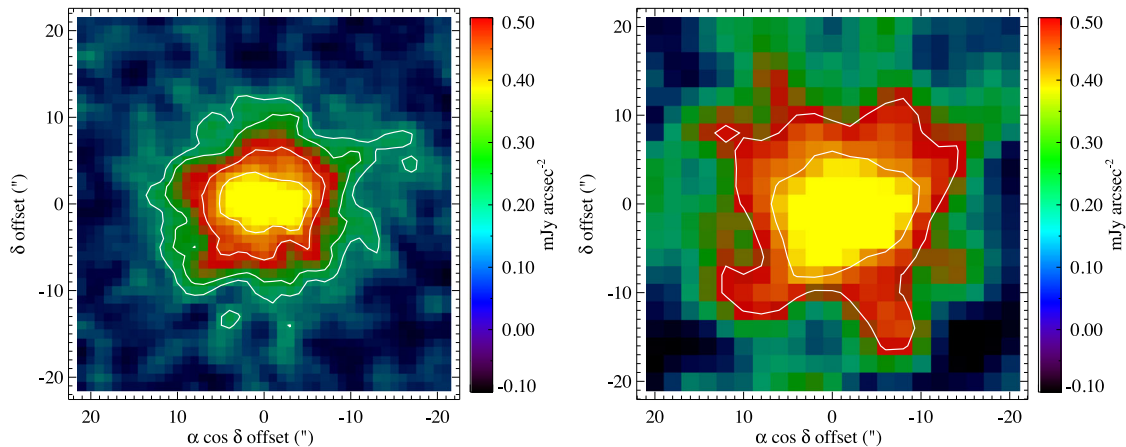


Figure 4. Star-subtracted images at 70 (left) and 160 μm (right). Here a PSF has been scaled to the photospheric flux in each band and subtracted from the images. Contours show 3σ , 5σ , 10σ , and 15σ significance levels of the remaining flux (only the 3σ and 5σ contours are visible in the bottom image).

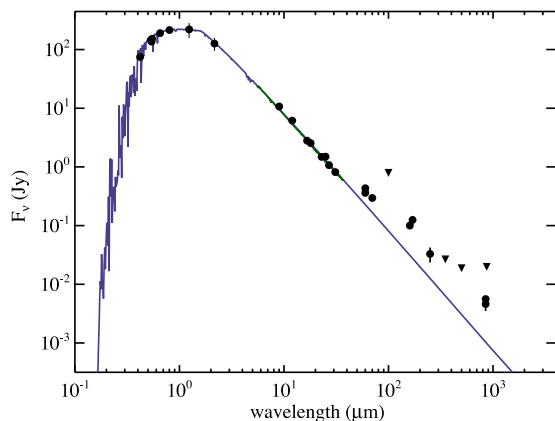


Figure 5. Observed SED of τ Ceti. Circles are measured fluxes, while triangles show upper limits. *Spitzer* IRS data are shown in green, on top of the photospheric model (blue line). The observed data include fluxes obtained from optical (Bessel 1990; Perryman & ESA 1997; Hauck & Mermilliod 1998; Høg et al. 2000; Mermilliod 2006), 2MASS (Skrutskie et al. 2006), *Spitzer* (Chen et al. 2006), *AKARI* (Ishihara et al. 2010), *IRAS* (Moshir et al. 1990), *ISO* (Habing et al. 2001), JCMT (Greaves et al. 2004, Greaves et al. in preparation), and HHT (Holmes et al. 2003), as well as the *Herschel* PACS and SPIRE values and upper limits. See Tables 2 and 3 for values.

significantly higher than those expected from the photosphere alone. For example, the observed 160 μm flux is 111 ± 8 mJy while the expected 160 μm flux from the photosphere is 31.1 ± 0.4 mJy.

The appearance of excess emission in the SED suggests that τ Ceti is indeed surrounded by cooler dust. The narrow wavelength range of the detected excess and the lack of widely extended PACS emission, however, put constraints on the location of this dust. On one hand, the fact that the excess is seen only at wavelengths longer than 24 μm suggests the dust is cold and thus situated at relatively large distances from the star. On the other hand, the small scale of the emission in the PACS images suggests the dust also cannot be too far from the star. In the following, we describe a simple debris disc model that remains consistent with the observed optical to mid-infrared emission, and that also can reproduce well the fluxes and extents of the observed far-infrared (PACS) emission.

3.1 Modelling the disc

We modelled the τ Ceti disc images and spectrum in a two-step process. The images provide all-important constraints on the spatial structure, which we obtain first by reproducing the PACS and SPIRE 250 μm images using a simple dust disc model (Section 3.1.1). This process does not yield definitive results because the PACS

Table 3. Observational data from the literature.

Band	λ (μm)	Obs. flux (Jy)	Uncertainty (Jy)	Citation
U_J	0.364	146.6	3.2	Mermilliod (2006)
B_T	0.42	74.7	1.1	Høg et al. (2000)
B_J	0.442	146.4	3.2	Mermilliod (2006)
V_T	0.532	145.7	1.4	Høg et al. (2000)
H_p	0.541	136.7	0.68	Perryman & ESA (1997)
V_J	0.547	151.9	3.2	Mermilliod (2006)
R_C	0.653	190.2	3.5	Bessel (1990)
I_C	0.803	214.9	3.9	Bessel (1990)
J	1.24	220.6	63	Cutri et al. (2003)
K_s	2.16	126.4	32	Cutri et al. (2003)
IRS1 ^a	6.5	18.15	0.65	Chen et al. (2006)
IRS2 ^a	8.69	10.19	0.24	Chen et al. (2006)
AKARI9	9	10.71	0.17	Ishihara et al. (2010)
IRS3 ^a	11.4	5.885	0.13	Chen et al. (2006)
IRAS12	12	6.158	0.42	Moshir et al. (1990)
IRS4 ^a	16.6	2.801	0.073	Chen et al. (2006)
AKARI18	18	2.544	0.071	Ishihara et al. (2010)
IRS5 ^a	22.9	1.509	0.039	Chen et al. (2006)
IRAS25	25	1.503	0.14	Moshir et al. (1990)
IRS6 ^a	27	1.094	0.025	Chen et al. (2006)
IRS7 ^a	31	0.8393	0.021	Chen et al. (2006)
ISO60	60	0.433	0.037	Habing et al. (2001)
IRAS60	60	0.3978	0.048	Moshir et al. (1990)
IRAS100	100	0.8253	0.27	Moshir et al. (1990)
ISO170	170	0.125	0.021	Habing et al. (2001)
SCUBA	850	0.0058	0.0006	Greaves et al. (2004)
SCUBA-2	850	0.005	0.001	Greaves et al. (in preparation)
HHT870	870	<0.0198	–	Holmes et al. (2003)

^a IRS values are binned from spectral data in Chen et al. (2006).

image resolutions limit what can be inferred about the disc inner edge. Using the results from the spatial modelling and an additional assumption of specific grain properties to model the disc spectrum (Section 3.1.2) yields further constraints on the disc inner edge.

3.1.1 Image-based disc model

We first use the PACS and SPIRE 250 μm images to fit a physical model for the disc structure. The 250 μm image has little spatial information, but we can measure the model flux as a check on the above photometry (finding 35 ± 10 mJy, larger than the 24 mJy estimated above if the disc were unresolved at 250 μm). Our spatial model has been used previously to model *Herschel*-resolved debris discs (e.g. Kennedy et al. 2012, 2013), and generates a high-resolution image of an azimuthally symmetric dust distribution with a small opening angle, as viewed from a specific direction. These models are then convolved with a PSF model (observations of calibration star α Tau) for comparison with the observed disc (Fig. 6). The best-fitting model is found using by-eye approximation followed by least-squares minimization. As the entire multi-dimensional parameter space was not searched, the model presented is not necessarily unique, but provides a good indication of the probable disc structure. By checking the fit of different parameter combinations, we were able to get a good feel for how well-constrained the different parameters are and feel we have converged on a good model, within observational errors.

Due to the limited resolution of the images of τ Ceti, our model disc is a simple power law in radial surface density ($\Sigma \propto r^\gamma$), which extends from r_{in} to r_{out} . This approach allows us to test whether or not the disc is radially extended. We use the simple assumption of a blackbody temperature law ($T = T_{1\text{au}} r^{-0.5}$, with $T_{1\text{au}}$ being the disc temperature at 1 au and radius r in au). Given that the disc temperature and surface density are degenerate without multiple well-resolved images, neither γ nor $T_{1\text{au}}$ is well constrained. Physically, $T_{1\text{au}}$ should be greater than about 230 K, because this is the temperature that grains with blackbody absorption and emission would have at 1 au from τ Ceti. Temperatures up to factors of 3–4 greater are possible if the emission comes primarily from small grains, which emit inefficiently at long wavelengths and have higher temperatures to maintain energy equilibrium (e.g. Booth et al. 2013).

The model also includes a background source to the east that is only visible in the 160 μm image. This does not significantly affect

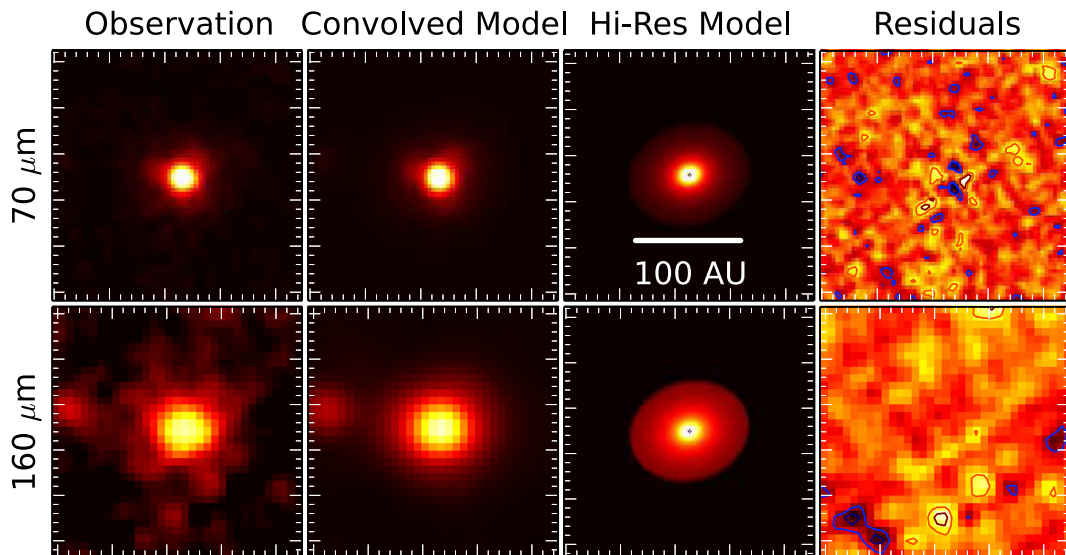


Figure 6. An example of a disc model that matches the *Herschel* images. Panels are on the same scale as Fig. 1, and a 100 au scale bar is shown for reference. Top panels show the *Herschel* data and model at 70 μm , lower panels at 160 μm . From left to right, panels show the *Herschel* data, the model convolved to the same resolution as the data, a high-resolution version of the model, and the residuals of data-model (-3σ , -2σ , 2σ , and 3σ contours). Some 3σ residuals are still visible in the 70 μm image; these are probably due to imperfect fitting of the beam (see text).

any of the parameters of the fit, but does allow us to better estimate the 250 μm disc flux.

To model the *Herschel* images of τ Ceti, we initially tried a simple narrow ring. We found that this model failed to reproduce the observed images and conclude that the emission is radially extended. We therefore allowed r_{in} and r_{out} , and γ , the surface density power-law exponent, to vary independently. The low surface brightness of the disc in the *Herschel* images limits our ability to constrain the disc model parameters. Primarily, a degeneracy between disc surface density profile, the inner edge location, and the dust temperature allowed a range of models to reproduce the data. For a $\gamma = -1$ model, the disc is centrally concentrated and the best-fitting inner edge is at about 10 au with $T_{1\text{au}} \sim 380$ K. For a flat profile ($\gamma = 0$) the disc is less centrally concentrated and the inner edge is closer, around 2 au (and $T_{1\text{au}}$ is the same). For a radially increasing surface density ($\gamma = 1$), the inner edge is around 3 au and $T_{1\text{au}} \sim 180$ K. We return to this issue when considering SED models that make assumptions about grain properties in Section 3.1.2.

The low surface brightness of the disc in the *Herschel* images limits our ability to constrain the disc model parameters. However, despite the degeneracies between $T_{1\text{au}}$, r_{in} and γ , the best-fitting models have similar inner radii of 2–3 au (with large uncertainty, acceptable fits range from roughly 1–10 au), and outer radii of $55 \text{ au} \pm 5 \text{ au}$. The disc may, however, extend to larger radii at a level undetectable by these observations. The disc geometry is constant across different models, with a disc inclination (i.e. from face-on) of 35° and position angle (East of North) of 105° . Using brute-force grid calculations we estimate that the 1σ uncertainty in these angles is about 10° .

Fig. 6 shows an example of a well-fitting model with $\gamma = 0$. Some residual structure is seen near the star at 70 μm , and very similar structure is seen for different models. We suspect it arises due to the brightness of τ Ceti itself; the high signal-to-noise ratio of the stellar emission means that the PSF model used (α Tau) must be a very good match to the PSF for the τ Ceti observation. Kennedy et al. (2012) showed that the PACS 70 μm PSF varies at the 10 percent level, which is a probable reason for the non-zero residuals near the star.

3.1.2 SED-based disc model

Though in general the shape of a modified blackbody provides a good approximation to the emission profile of dust grains, it cannot tell us much about the properties of the grains. A better approximation of the dust grains can be found by taking into account their optical properties and the size distribution of dust in the disc. Accordingly, we follow the model described in Wyatt & Dent (2002) and similarly assume non-porous, amorphous silicate grains with an organic refractory mantle. The silicate core makes up 1/3 of the grains, which have an amorphous carbon coating. Grains are assumed to be spherical, and absorption efficiencies are calculated using the Mie theory, Rayleigh–Gans theory, or geometric optics in the appropriate limits (see also Li & Greenberg 1997). We assume these grains follow a size distribution power law of $n(D)dD \propto D^{-3.5}dD$ from a minimum grain size, D_{min} , to an arbitrarily large grain size (Dohnanyi 1969). Many of the properties of the grain model are degenerate. For instance, a shallower size distribution has the same effect as increasing the minimum grain size, and the exact composition of the grains cannot easily be determined without spectral features. For this reason, we only varied D_{min} and the inner edge of the disc (since this was poorly constrained from the image-based

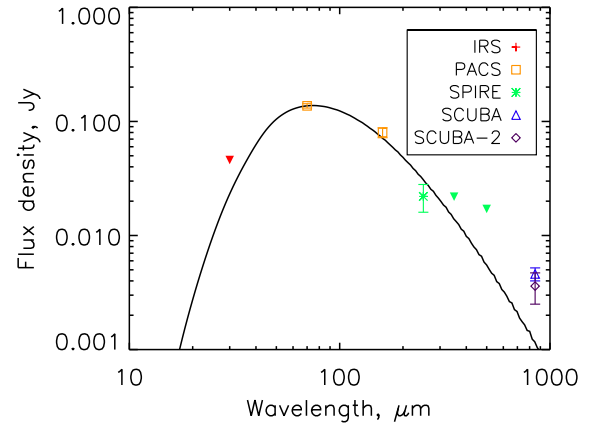


Figure 7. Fitting the SED with a realistic grain model, using a flat surface density profile ($\gamma = 0$). The *Herschel* PACS and SPIRE 250 μm data points are used in the fit, along with upper limits from *Spitzer* IRS and *Herschel* SPIRE 350 μm and 500 μm . SCUBA and SCUBA-2 850 μm data are also shown, but are not used in the fit. See legend for symbols.

modelling). We also tested two values of the surface density power law, γ equal to 0 and 1 since this quantity is also poorly constrained from the image-based modelling.

No SED model can be found that fits both the SCUBA and PACS 160 μm photometry, suggesting that a separate, cooler disc component may be required to fully explain the sub-mm observations, since a slope that fits both these points is too shallow to even be fit by a perfect blackbody. Further investigation of the multi-epoch SCUBA and SCUBA-2 data is left to Greaves et al. (in preparation).

For the following we therefore focus on fitting the model to the PACS data, the SPIRE data and the upper limit from the *Spitzer* IRS spectral data. We find the best-fitting model to have a flat surface density profile ($\gamma = 0$), a minimum grain diameter of $15 \pm 8 \mu\text{m}$ and an inner radius of 6_{-4}^{+15} au (parameter uncertainties calculated using a χ^2 cut). The best fit is shown in Fig. 7. There is some anti-correlation between the minimum diameter and inner radius such that models with a larger inner radius require a smaller minimum grain size. Models with a rising surface density of $\gamma = 1$ can still plausibly fit the photometry with a minimum grain size of 8 μm and an inner radius between 1 and 17 au, although this provides a poorer fit to the data.

Unfortunately, these SED models were not very sensitive to different disc inner edges, and the results of this modelling technique, while agreeing with the results of the image-based model, did not provide any stronger constraints on the inner edge of the disc.

3.1.3 Disc properties inferred from both models

To summarize the findings of both models, τ Ceti’s disc extends from a radius similar to the inner Solar system (~ 1 –10 au) to just outside the distances inhabited by the main classical Kuiper Belt.

The image-based model’s uncertainty in the inner edge locations arises from the variations in the 70 μm beam shape and the resolution limits in both PACS wavelengths. The uncertainty in the inner edge as predicted by the SED-based model can be attributed to the calibration uncertainties in the *Spitzer* IRS spectrum and a small number of photometric measurements of the excess, while the outer edge uncertainty is mainly due to the low surface brightness in the PACS 160 μm image.

We do not give a mass estimate for our dust models, as the uncertainties due to assumptions about the grains give disc masses

that vary by orders of magnitude. The most accurate disc masses come from submillimeter fluxes, temperatures, and opacities, thus we leave calculation of the disc mass in the τ Ceti system to the forthcoming SCUBA and SCUBA-2 analysis (Greaves et al., in preparation)

In the next section, we will use the (limited) constraints imposed by the disc to investigate the validity of a proposed planetary system.

4 τ CETI'S POSSIBLE PLANETARY SYSTEM

Though previous studies failed to find planets around τ Ceti using the RV technique (e.g. Pepe et al. 2011), Tuomi et al. (2013) report evidence for a five-planet system after extensive modelling and Bayesian statistical analysis using combined RV data from three different planet surveys.

The most likely system found by Tuomi et al. consists of five super-Earths, ranging in mass ($M \sin i$) from 2.0 to 6.6 M_{\oplus} , with small-to-moderate eccentricities (~ 0 –0.2), in a tightly packed configuration with semimajor axes ranging from 0.105 to 1.35 au. Tuomi et al. (2013) show that their system is stable based on Lagrange stability thresholds, but do not perform detailed numerical integrations.

We note that the periodic RV signals detected by Tuomi et al. (2013) were only interpreted as planets by these authors with caution; it is possible that the signals are from another source, such as stellar activity or instrumental bias, although there is no direct evidence in favour of these alternative interpretations either. In this section we investigate the stability of the proposed planet system, and assuming that the planetary system is real, use it to place constraints on the inner disc edge using dynamical simulations.

4.1 System inclination

Since the planets' existence was surmised using RV data, we have no direct information on the inclination of the planetary system. In addition to the coplanar precedent of our own Solar system, several recent studies find evidence that star–planet–disc systems without hot Jupiters should be well-aligned. For example, Kennedy et al. (2013) discuss the HD 82943 system, where the star, planets, and debris disc have well-measured inclinations, and are all coplanar within $\sim 10^\circ$. Furthermore, Greaves et al. (2014) find that, out of 11 systems with *Herschel*-resolved discs and well-measured stellar inclinations, all are consistent with being coplanar. Watson et al. (2011) measure the rotational axes of stars with resolved debris discs, and reach the same conclusion. Studies of *Kepler*-discovered multiplanet systems (Hirano et al. 2012; Sanchis-Ojeda et al. 2012; Albrecht et al. 2013; Chaplin et al. 2013) also have found that the orbital planes of the planetary systems tend to be well-aligned with the equators of the host stars. We believe these studies provide ample evidence that compact, low-mass planetary systems like τ Ceti are usually well-aligned systems.

Greaves et al. (2004) used the low rotational velocity measured by Saar & Osten (1997) as evidence that we are viewing τ Ceti within 40° of pole-on, which was inconsistent with their measurements of the disc inclination. However, at the SCUBA resolution and wavelength, background confusion made it difficult to measure the disc inclination. The analysis of the *Herschel* images presented here has made it clear that the disc is close to face-on, consistent with being aligned with the equatorial plane of τ Ceti.

Assuming the best-fitting inclination for the disc ($\sim 30^\circ$) equals the inclination for τ Ceti and its planetary system, the best-fitting values of $M \sin i$ given in Tuomi et al. (2013) should be doubled. As

Table 4. Properties of a stable planet system around τ Ceti.

Planet	M^a (M_{\oplus})	a (au)	e
a	4.0	0.105	0.16
b	6.2	0.195	0.03
c	7.2	0.374	0.08
d	8.6	0.552	0.05
e	13.2	1.35	0.03

^aPlanet masses are given assuming $i_{\text{sys}} = 30^\circ$.

found in Section 4.2.1, such masses still allow a dynamically stable configuration for the planets. Table 4 gives the masses, semimajor axes, and eccentricities for this system. We note that, however, this is only one possible configuration of planets that satisfies both the requirement of long-term stability and the Bayesian analysis of Tuomi et al. (2013).

4.2 Dynamical simulations

We perform numerical simulations using SWIFT-RMVS4 (Levison & Duncan 1994), with a time-step of 0.002 years (0.73 d). This allows > 15 time-steps per orbit for accurate calculation of the positions of all five planets, including the innermost planet, with an orbital period of only 14 d. All of our simulations were carried out on the Canadian Advanced Network for Astronomical Research (CANFAR; Gaudet et al. 2009).

For our dynamical simulations, we ignore the mass of the disc since the largest reasonable estimate of τ Ceti's disc mass is about 10 per cent of the mass of the outermost planet ($M_{\text{disc}} \simeq 1M_{\oplus}$; Greaves et al. 2004). While Moore & Quillen (2013) find that a disc mass this high relative to the planet masses can affect the dynamical stability lifetime of a planetary system, the system they modelled (HR 8799) extends to much larger separations from the star than that of τ Ceti. HR 8799b, the outermost planet in the system, has a semimajor axis of 68 au (Marois et al. 2008) and the planetesimal disc extends from 100 to 310 au (Matthews et al. 2014). If the HR 8799 system is scaled down so that the orbit of HR 8799b matches the outermost planet in the τ Ceti system, HR 8799's entire debris disc would extend to only ~ 3 –6 au, while in reality, τ Ceti's disc mass is actually spread out to ~ 55 au. Given the small semimajor axes of all the planets in the τ Ceti system, we therefore believe the contribution of the disc mass to the stability of the system is negligible.

We performed two types of simulations: planetary system stability and disc orbit stability. Planet stability simulations were run for 100 Myr, corresponding to over two billion orbits of the innermost planet, while disc simulations were run for 10 Myr with many massless test particles included in addition to the five planets to diagnose stable orbits for small bodies. Planetary systems were deemed unstable if any planet's semimajor axis changes by > 1 per cent over the course of an integration. The same change in semimajor axis is used to diagnose stable versus unstable disc particle orbits.

Given the infinite range of possible starting conditions for this multiplanet system, we chose a few representative possibilities and investigated the stability of those before proceeding to disc simulations. We found the highest eccentricities allowed by the statistical analysis of Tuomi et al. (2013) yielded unstable planetary systems. The more moderate (best-fitting) eccentricities and very low eccentricities result in planetary systems stable on time-scales of 100 Myr,

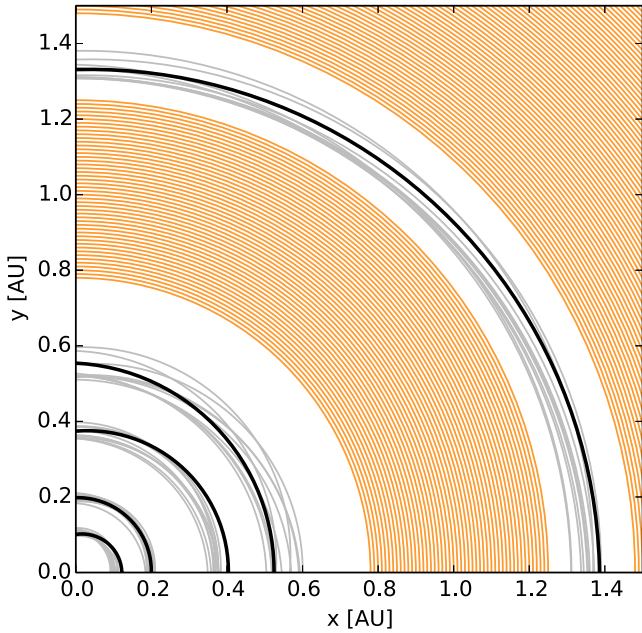


Figure 8. Initial (coplanar) orbits of five planets are shown in black, using masses and orbital elements as given in Table 4. Orbital elements which were unconstrained by the Tuomi et al. (2013) analysis (Ω , ω , and \mathcal{M}) are chosen at random. Grey lines show how the orbits evolve over the course of a 100 Myr integration. Stable disc particle orbits (surviving a 10 Myr integration) are shown in orange.

even when planet masses are increased by a factor of $1/\sin i_{\text{sys}}$, up to inclinations out of the sky plane as low as 5° , nearly perpendicular to our line of sight.

4.2.1 Disc simulations

After confirming that the planetary system is stable over a reasonable range of possible orbital configurations, we use one stable planetary system (Table 4) as part of another set of simulations. Here we quantify the stability of small body orbits near planets in order to find where the debris disc would be stable over long time-scales. The small bodies are represented by massless test particles in these simulations.

The fairly small planets of the τ Ceti system are on close-to-circular orbits and so they do not clear large annuli. Using just the best-fitting parameters of the five planets from Tuomi et al. (2013) results in stable disc particle orbits all the way down to 0.1 au separation from the orbit of the outermost planet (at 1.35 au). Fig. 8 shows that stable disc orbits also exist in the gap between the outermost two planets.

4.2.2 Simulations with an additional planet

One way to constrain the inner disc edge at greater distances from the star is to assume that there is an additional planet in the system further from the host star and to estimate the properties of this hypothetical companion based on the available data. Although this scenario was not specifically tested in the work of Tuomi et al. (2013), the RV data sets could not be expected to be very sensitive to planets with masses of roughly that of Neptune on longer period (>5 yr) orbits.

In Fig. 9, we show the estimated detection threshold of additional planets orbiting the star based on the RV data analysis of Tuomi

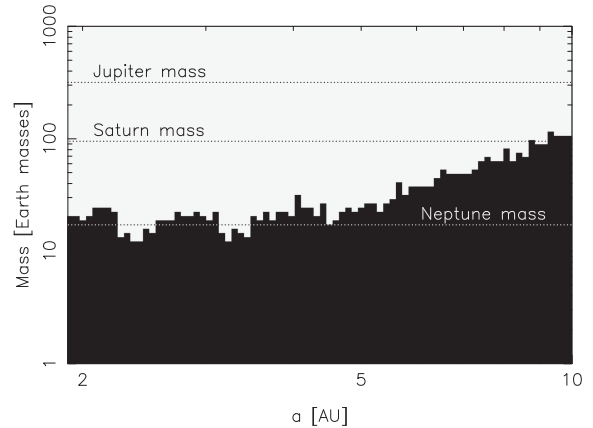


Figure 9. Black region shows planet mass (with the $\sim 30^\circ$ system inclination taken into account) and semimajor axis combinations that would not be detectable using the analysis methods of Tuomi et al. (2013). White region shows mass–semimajor axis combinations which cannot exist in the τ Ceti system based on current RV data.

et al. (2013). The area in the mass–period space where additional planet candidates are ruled out (white area) has been estimated by assuming there is an additional planet with a semi-major axis in excess of those of the previously proposed candidates. This estimation was performed by drawing a sample from the posterior probability density of the parameters of the sixth planet in a model that extends in the semi-major axis space from a minimum of 1.8 au to a maximum value that we have chosen to be 10 au, the outermost bound of the inner disc edge consistent with the *Herschel* data. The computations are performed as in Tuomi et al. (2014), and we have assumed that the planetary eccentricity has a prior probability density that penalizes high eccentricities as they approach unity, because the eccentricities of low-mass planets appear to follow such a distribution (Tuomi & Anglada-Escudé 2013).

It is worth noting that Jupiter-mass planets within 10 au would have already been detected by previous RV studies (e.g. Pepe et al. 2011, see also analysis by Cumming et al. 2008). Using the analysis described above, Fig. 9 shows that we can push to lower planetary masses, ruling out the existence of planets of Neptune-mass or larger within orbital distances of 5 au, and excluding the possibility that Saturn-mass or larger planets exist in the system inside 10 au.

We ran simulations with a sixth planet having twice Neptune’s mass on circular orbits at 5–10 au, and find that these systems are stable on long time-scales (100 Myr).

While the disc could be cleared to large semimajor axes by a more eccentric outer planet orbit, this situation would destabilize the inner five planets within millions of years at most. Using a circular orbit for the outermost planet constrains the stable disc particle orbits to just outside a few times the planet’s Hill radius, as expected. While it is exciting to consider the possibility of additional planets in the system, an additional planet with less than a Saturn mass (outside 5 au) or less than a Neptune mass (inside 5 au) would constrain the inner edge of the disc to larger distances from the star. With the large uncertainties on inner edge of the disc, however, this additional layer of complexity is unwarranted. Future high-resolution images of the inner edge of τ Ceti’s disc will provide much-needed constraints on the actual location of the inner disc edge, and continued RV observations may detect additional, more distant planets.

5 DISCUSSION

5.1 Properties of the τ Ceti disc

Herschel observations have confirmed the existence of the resolved debris disc originally imaged by Greaves et al. (2004), though the inclination we measure is $\sim 30^\circ$ from face-on, which is different than the nearly edge-on alignment first reported from the analysis of the SCUBA images. Modelling the disc gives some weak constraints on the extent of the disc, which extends roughly 2–55 au from τ Ceti. There is no significant structure observed in the disc, and using a realistic dust grain spectrum (as opposed to blackbody) provided only moderately better constraints on the inner edge of the disc. Additional photometric or spectral data at far-IR wavelengths would be valuable for constraining dust grain properties in this system.

5.2 Disc inner edge

The current data do not constrain the inner disc edge very strongly. While an inner edge at 2–3 au is consistent with both the SED- and image-based models, neither can formally rule out a disc extending as close to the star as 1 au, well into the realm which may be populated by planets, or as far from the star as 10 au, allowing dynamical room for one or more additional planets.

We note that interferometric near-IR measurements have been made of the τ Ceti system using the CHARA array (di Folco et al. 2007). They found they could reproduce the near-IR excess using a population of small ($< 1 \mu\text{m}$) dust grains extending from the limits of their observation field to extremely close to the star (3 au to ~ 0.1 au), which overlaps with the region where the planets may exist. However, the mass in dust grains is extremely small ($\sim 10^{-9} M_\oplus$), comparable to the mass of zodiacal (asteroidal) dust in our Solar system (Hahn et al. 2002). Models show that dust produced by collisions at larger distances can inspiral (due to the Poynting–Robertson drag) past planets in the inner Solar system with little disruption other than longer time spent inside planetary mean-motion resonances (Nesvorný et al. 2011). For this reason, the presence of this tenuous dust in the inner portions of the τ Ceti system does not rule out the planets.

The exquisite resolving power of ALMA should be able to image the inner edge of the main dust belt easily, and that will clarify which of three possibilities is true:

- (1) The disc extends well into the planetary regime (< 1.35 au), which would be serious evidence against the planets proposed by Tuomi et al. (2013).
- (2) The disc edge is close to the orbit of the outermost planet (> 1.35 au and < 2.0 au) and the proposed five-planet system is enough to constrain the disc edge.
- (3) The disc edge ends significantly far away from the outermost planet (> 2.0 au), in which case another process must be invoked to explain the edge (e.g. another planet, or possibly collisional processes).

ALMA will also be more sensitive to larger dust grains that more closely trace the positions of the parent bodies that are collisionally grinding to make the smaller dust grains observed at mid- and far-IR wavelengths. The high-resolution of ALMA will also illuminate whether the dust in the τ Ceti debris annulus is produced by a narrow ‘birth ring’ as has been observed in other debris disc systems (e.g. AU Mic; Wilner et al. 2012; MacGregor et al. 2013).

5.3 The disc–planet relationship

If confirmed, τ Ceti’s low-mass multiplanet system would fit with the results of simulations by Raymond et al. (2011) and extend the trend observed by Wyatt et al. (2012): the presence of exclusively low-mass planetary systems ($< M_{\text{Saturn}}$) and far-IR excess ($\sim 70 \mu\text{m}$) is strongly correlated for mature host stars.

These models hint that systems with planets of mass $> M_{\text{Jup}}$ are inherently unstable in their early days (e.g. Raymond et al. 2012). We know from the structure of the Kuiper Belt that the four giant planets in our own Solar system have migrated, and that a much more massive primordial Kuiper Belt is required to fuel this migration (e.g. Gomes et al. 2005). It may be that the debris disc around solar analogue τ Ceti is brighter and more massive than the Kuiper Belt because there are no giant planets in the system to migrate and disrupt the primordial planetesimal disc.

Unfortunately, the *Herschel* images do not provide very tight constraints on the presence of gaps or clumps in the disc that may be due to perturbations by massive planets.

Resonant and secular perturbations by a planet on a disc can produce telltale clumps and gaps in the dust disc, but the grain sizes that are most visible at $70 \mu\text{m}$ and $160 \mu\text{m}$ will be smeared out by radiation forces relative to the larger (\sim millimeter-sized) dust grains and parent planetesimals, making these clumps much harder or even impossible to detect (Wyatt 2006). In addition, predicting clumps that may be present in the τ Ceti disc via numerical modelling of secular perturbations and mean-motion resonances in the planetesimal disc by the planets is not currently feasible. These perturbations are quite sensitive to the masses and exact orbits of the planets, which have very large uncertainties or are even completely unconstrained, as in the case of the angular orbital elements.

As shown in Section 3.1.1, the *Herschel* images are best reproduced using a smooth disc model, with no structure. However, because of the large beam size, this is not a very strong constraint on the smoothness of the disc. A several au-wide gap could easily be missed due to the *Herschel* resolution. In order for a clump in the disc to be detectable, it would have to contain more than ~ 10 per cent of the total disc flux, based the sensitivities quoted in Table 2.

In order to rule out clumps or gaps in the disc with any degree of certainty, high-resolution, long wavelength observations are required in order to probe the distribution of large dust grains that are relatively unaffected by radiation forces. Within the next few months, ALMA observations will be used to probe the inner portions of the τ Ceti disc and provide some constraints both on the location of the inner edge of the disc and on the smoothness of the disc, which in turn will provide limits on the mass and orbital properties of undetected massive planets in the system, independent of the RV data.

6 SUMMARY AND CONCLUSIONS

τ Ceti hosts a bright debris disc that has been resolved by *Herschel*. The disc is uniform and symmetric, with a most likely inner edge at 2–3 au (though inner edges 1–10 au are not ruled out by the *Herschel* data) and an outer edge at 55 ± 10 au. It is inclined from face-on by $35^\circ \pm 10^\circ$ and can be fit by a surface density distribution of dust that increases linearly with distance from the star.

The proposed five-planet system is not ruled out by the disc model, and our dynamical simulations show that this system is stable for moderate planetary eccentricities. If the outermost planet is what constrains the inner edge of the disc, the inner edge should be at ~ 1.5 au. If there is an additional, as-yet undetected planet

(which is possible if its mass is below that of Neptune), it could be constraining the inner disc radius farther away from the star.

It appears that there are no Jupiter-mass planets inside 10 au in the τ Ceti system, so the comparison to our Solar system may not be so appropriate. If the proposed planets are real, the τ Ceti system is composed of small rocky planets close to the star with a disc extending from the inner Solar system out to Kuiper Belt-like distances from the star, perhaps resembling our Solar system if the giant planets had failed to form and the primordial planetesimal disc had not been disrupted by planet migration. Future high-resolution observations are required to constrain the edges of the disc, and to confirm the planetary system.

ACKNOWLEDGEMENTS

The authors thank an anonymous referee for providing helpful comments on this paper. SML and BCM acknowledge an NSERC Discovery Accelerator Supplement which funded this work. This work was also supported by the European Union through ERC grant number 279973 (GMK). MB acknowledges support from a FONDECYT Postdoctoral Fellowship, project no. 3140479.

REFERENCES

- Albrecht S., Winn J. N., Marcy G. W., Howard A. W., Isaacson H., Johnson J. A., 2013, *ApJ*, 771, 11
- Aumann H. H., 1985, *PASP*, 97, 885
- Bessel M. S., 1990, *A&AS*, 83, 357
- Booth M. et al., 2013, *MNRAS*, 428, 1263
- Chaplin W. J. et al., 2013, *ApJ*, 766, 101
- Chen C. H. et al., 2006, *ApJS*, 166, 351
- Cumming A., Butler R. P., Marcy G. W., Vogt S. S., Wright J. T., Fischer D. A., 2008, *PASP*, 120, 531
- Cutri R. M. et al., 2003, *VizieR Online Data Catalog*, 2246, 0
- di Folco E. et al., 2007, *A&A*, 475, 243
- Dohnanyi J. S., 1969, *J. Geophys. Res.*, 74, 2531
- Gaudet S., Dowler P., Goliath S., Hill N., Kavelaars J. J., Peddle M., Pritchett C., Schade D., 2009, in Bohlender D. A., Durand D., Dowler P., eds, *ASP Conf. Ser. Vol. 411. Astronomical Data Analysis Software and Systems XVIII*. Astron. Soc. Pac., San Francisco, p. 185
- Gomes R., Levison H. F., Tsiganis K., Morbidelli A., 2005, *Nature*, 435, 466
- Greaves J. S., Wyatt M. C., Holland W. S., Dent W. R. F., 2004, *MNRAS*, 351, L54
- Greaves J. S. et al., 2014, *MNRAS*, 438, L31
- Griffin M. J. et al., 2010, *A&A*, 518, L3
- Habing H. J. et al., 2001, *A&A*, 365, 545
- Hahn J. M., Zook H. A., Cooper B., Sunkara B., 2002, *Icarus*, 158, 360
- Hauck B., Mermilliod M., 1998, *A&AS*, 129, 431
- Hirano T. et al., 2012, *ApJ*, 759, L36
- Holland W. S. et al., 1999, *MNRAS*, 303, 659
- Holmes E. K., Butner H. M., Fajardo-Acosta S. B., Rebull L. M., 2003, *AJ*, 125, 3334
- Høg E. et al., 2000, *A&A*, 355, L27
- Ishihara D. et al., 2010, *A&A*, 514, A1
- Kennedy G. M., Wyatt M. C., Sibthorpe B., Phillips N. M., Matthews B. C., Greaves J. S., 2012, *MNRAS*, 426, 2115
- Kennedy G. M., Wyatt M. C., Bryden G., Wittenmyer R., Sibthorpe B., 2013, *MNRAS*, 436, 898
- Lagrange A. M. et al., 2010, *Science*, 329, 57
- Levison H. F., Duncan M. J., 1994, *Icarus*, 108, 18
- Li A., Greenberg J. M., 1997, *A&A*, 323, 566
- MacGregor M. A. et al., 2013, *ApJ*, 762, L21
- Mamajek E. E., Hillenbrand L. A., 2008, *ApJ*, 687, 1264
- Marois C., Macintosh B., Barman T., Zuckerman B., Song I., Patience J., Lafrenière D., Doyon R., 2008, *Science*, 322, 1348
- Matthews B., Kennedy G., Sibthorpe B., Booth M., Wyatt M., Broekhoven-Fiene H., Macintosh B., Marois C., 2014, *ApJ*, 780, 97
- Mermilliod J. C., 2006, *VizieR Online Data Catalog*, 2168, 0
- Moore A., Quillen A. C., 2013, *MNRAS*, 430, 320
- Moshir M. et al., 1990, *BAAS*, 22, 1325
- Mouillet D., Larwood J. D., Papaloizou J. C. B., Lagrange A. M., 1997, *MNRAS*, 292, 896
- Müller T., Nielbock M., Balog Z., Klaas U., Vilenius E., 2011, *PACS Observers Manual*, Vol. 708, p. 1728, available online at: http://herschel.esac.esa.int/Docs/PACS/html/pacs_om.html
- Nesvorný D., Janches D., Vokrouhlický D., Pokorný P., Bottke W. F., Jenniskens P., 2011, *ApJ*, 743, 129
- Ott S., 2010, in Mizumoto Y., Morita K. I., Ohishi M., eds, *ASP Conf. Ser. Vol. 434. Astronomical Data Analysis Software and Systems XIX*. Astron. Soc. Pac., San Francisco, p. 139
- Pepe F. et al., 2011, *A&A*, 534, A58
- Perryman M. A. C. *ESAeds*, 1997, *The HIPPARCOS and TYCHO Catalogues. Astrometric and Photometric Star Catalogues derived from the ESA HIPPARCOS Space Astrometry Mission*, Vol. 1200 ESA Special Publication
- Pilbratt G. L. et al., 2010, *A&A*, 518, L1
- Poglitsch A. et al., 2010, *A&A*, 518, L2
- Raymond S. N. et al., 2011, *A&A*, 530, A62
- Raymond S. N. et al., 2012, *A&A*, 541, A11
- Saar S. H., Osten R. A., 1997, *MNRAS*, 284, 803
- Sanchis-Ojeda R. et al., 2012, *Nature*, 487, 449
- Skrutskie M. F. et al., 2006, *AJ*, 131, 1163
- Spiegel D. S., Burrows A., 2012, *ApJ*, 745, 174
- Swinyard B. M. et al., 2010, *A&A*, 518, L4
- Tuomi M., Anglada-Escudé G., 2013, *A&A*, 556, A111
- Tuomi M. et al., 2013, *A&A*, 551, A79
- Tuomi M., Jones H. R. A., Barnes J. R., Anglada-Escudé G., Jenkins J. S., 2014, *MNRAS*, 441, 1545
- van Leeuwen F., 2007, *A&A*, 474, 653
- Vandenbussche B. et al., 2010, *A&A*, 518, L133
- Watson C. A., Littlefair S. P., Diamond C., Collier Cameron A., Fitzsimmons A., Simpson E., Moulds V., Pollacco D., 2011, *MNRAS*, 413, L71
- Wilner D. J., Andrews S. M., MacGregor M. A., Hughes A. M., 2012, *ApJ*, 749, L27
- Wyatt M. C., 2006, *ApJ*, 639, 1153
- Wyatt M. C., Dent W. R. F., 2002, *MNRAS*, 334, 589
- Wyatt M. C. et al., 2012, *MNRAS*, 424, 1206

¹*Department of Physics & Astronomy, University of Victoria, PO Box 1700, STN CSC, Victoria, BC V8W 2Y2, Canada*

²*National Research Council of Canada, Herzberg Astronomy & Astrophysics Program, 5071 West Saanich Road., Victoria, BC V9E 2E7, Canada*

³*Institute of Astronomy, Cambridge University, Madingley Road, Cambridge CB3 0HA, UK*

⁴*SRON Netherlands Institute for Space Research, NL-9747 AD Groningen, the Netherlands*

⁵*Instituto de Astrofísica, Pontificia Universidad Católica de Chile, Vicuña Mackenna 4860, 7820436 Macul, Santiago, Chile*

⁶*Institute of Astronomy KU Leuven, Celestijnenlaan 200D, B-3001 Leuven, Belgium*

⁷*UK Astronomy Technology Centre, Royal Observatory Edinburgh, Blackford Hill, Edinburgh EH9 3HJ, UK*

⁸*Institute for Astronomy, University of Edinburgh, Royal Observatory Edinburgh, Blackford Hill, Edinburgh EH9 3HJ, UK*

⁹*SUPA, School of Physics and Astronomy, University of St. Andrews, North Haugh, St. Andrews KY16 9SS, UK*

¹⁰*Harvard-Smithsonian Center for Astrophysics, 60 Garden Street, Cambridge, MA 02138, USA*

¹¹*Centre for Astrophysics Research, University of Hertfordshire, College Lane, AL10 9AB Hatfield, UK*

¹²*Departamento de Astronomia, Universidad de Chile, Camino del Observatorio 1515, Las Condes, Santiago, Chile*

¹³*Astronomy and Astrophysics Research Group, Department of Physics and Astrophysics, Vrije Universiteit Brussel, Pleinlaan 2, B-1050 Brussels, Belgium*

¹⁴*Flemish Institute for Technological Research (VITO), Boeretang 200, B-2400 Mol, Belgium*

¹⁵*Department of Astronomy, Stockholm University, AlbaNova University Center, SE-10691 Stockholm, Sweden*

¹⁶*Stockholm University Astrobiology Centre, SE-106 91 Stockholm, Sweden*

¹⁷*Anton Pannekoek Institute, University of Amsterdam, Science Park 904, NL-1098 XH Amsterdam, the Netherlands*

¹⁸*Department of Astrophysics/IMAPP, Radboud University Nijmegen, PO Box 9010, NL-6500 GL Nijmegen, the Netherlands*

¹⁹*Institute of Planetary Research, German Aerospace Center, Rutherfordstrasse 2, D-124 89 Berlin, Germany*

²⁰*Leiden Observatory, University of Leiden, PO Box 9513, NL-2300 RA, Leiden, the Netherlands*

²¹*School of Physics and Astronomy, Cardiff University, Queens Buildings, The Parade, Cardiff CF24 3AA, UK*

²²*Scientific Support Office, Science and Robotic Exploration Directorate, ESA/ESTEC, Keplerlaan 1, NL-2200 AG Noordwijk, the Netherlands*

²³*European Southern Observatory, Karl Schwarzschild Strasse 2, D-85748 Garching, Germany*

²⁴*Institute for Astronomy, University of Edinburgh, Blackford Hill, Edinburgh EH9 3HJ, UK*

This paper has been typeset from a $\text{\TeX}/\text{\LaTeX}$ file prepared by the author.